Nominal vs. Effective Wake Fields and their Influence on Propeller Cavitation Performance

Regener, Pelle Bo; Mirsadraee, Yasaman ; Andersen, Poul

Published in:
Proceedings of the Fifth International Symposium on Marine Propulsors - smp'17

Publication date:
2017

Document Version
Peer reviewed version

Fifth International Symposium on Marine Propulsors
smp'17, Espoo, Finland, June 2017

Nominal vs. Effective Wake Fields and their Influence on Propeller Cavitation Performance

Pelle Bo Regener[1], Yasaman Mirsadraee[1,2], and Poul Andersen[1]

[1]Technical University of Denmark (DTU), Department of Mechanical Engineering, Lyngby, Denmark
[2]MAN Diesel & Turbo, Frederikshavn, Denmark

ABSTRACT

Propeller designers often need to base their design on the nominal model scale wake distribution, because the effective full scale distribution is not available. The effects of such incomplete design data on cavitation performance is examined in this paper. The behind-ship cavitation performance of two propellers is evaluated, where the cases considered include propellers operating in the nominal model and full scale wake distributions and in the effective wake distribution, also in model and full scale. The method for the analyses is a combination of RANS for the ship hull and a panel method for the propeller flow, with a coupling of the two for the interaction of ship and propeller flows. The effect on sheet cavitation due to the different wake distributions is examined for a typical full-form ship. Results show considerable differences in cavitation extent, volume, and hull pressure pulses.

Keywords

Propeller Cavitation, Wake Scaling, Effective Wake, RANS-BEM Coupling

1 INTRODUCTION

1.1 Motivation

Propeller cavitation is strongly influenced by the non-uniform inflow to the propeller. As the ship wake is dominated by viscous effects, it is subject to major scale effects. Still, propeller designers are generally only provided with the nominal wake field measured at model scale. This then needs to be scaled to match the estimated full scale effective wake fraction from a self-propulsion test to ensure that the average axial velocity in the propeller disk corresponds to the average effective inflow. However, scaling the field uniformly will not result in the right velocity distribution. In addition to the scale effects, the actual inflow field to the propeller is not the nominal field, but the effective wake field, including hull-propeller interaction. As a result, the propeller designer might base design decisions on insufficiently accurate information.

A successful propeller design is a trade-off between propeller cavitation performance and total propeller efficiency. The ability to predict cavitation performance at early design stages will eliminate the need for overly conservative designs. This paper intends to highlight the role of the wake field in the design, analysis, and optimization of a conventional ship propeller.

1.2 Background

Due to the higher Reynolds number at full scale compared to model scale, the boundary layer around the ship hull changes and hence the velocity distribution near the hull is altered. This difference results in a narrower wake peak and a lower wake fraction in full scale. The presence of the propeller behind the ship adds to the complexity of the problem because the propeller-hull interaction modifies the inflow field to the propeller as well.

Single-screw ship wake fields are usually characterized by a strongly non-uniform distribution of velocities with a wake peak at the 12 o'clock position, where the axial velocities are particularly low. This means that the blade sections of a propeller operating behind the ship experiences strong variations in angle of attack. As the hydrostatic pressure acting on the blade reaches its minimum at the same time as the blade experiences high angles of attack while passing the wake peak, this region of the wake field is particularly critical in terms of cavitation.

Analyzing the different factors influencing propeller cavitation and related erosion and vibration issues, an ITTC propulsion committee (Jessup et al., 2002) pointed out that for large container ships with highly-loaded propellers the wake field characteristics – and not propeller geometry details – are the key to achieving decent propeller cavitation performance.

Especially the depth of the wake peak, i.e. the difference between the lowest axial velocity occurring there and the maximum velocity in the propeller disk, is of decisive importance for the cavitation performance of a propeller behind

the ship. When uniformly scaling the nominal wake velocities to match the effective wake fraction, the width and depth of the wake peak are unlikely to be represented properly.

As this has been known for many years, different methods exist for estimating the full scale wake field of a ship, covering a rather wide range of complexity and sophistication. Usually the nominal wake field, measured at model scale, serves as input for these methods. A review of the most commonly used scaling methods was carried out some years ago by an ITTC specialist committee on wake field scaling (Fu et al., 2011). That report mentions the simplest form of wake scaling, where one only scales the wake field by changing the magnitude of the velocities uniformly to match a target wake fraction, as already described above. In that case the isolines of the input field (usually the measured nominal wake field) remain unchanged. Therefore, even calling this procedure a "scaling method" is questionable. While the shortcomings of this approach are well-known, it still appears to be commonly used for its simplicity.

Adding complexity while still only requiring very limited effort, the semi-empirical scaling method described by Sasajima & Tanaka (1966) decomposes the wake into a frictional and potential component and contracts the frictional wake based on horizontal velocity profiles. This still-popular method was recommended (with warnings) by above-mentioned ITTC committee in 2011 for the case when full scale wake data are not available.

Gaggero et al. (2014) compared the cavitation performance of conventional propellers in nominal full scale wake fields from CFD calculations to the performance in nominal full scale wake fields obtained by applying an empirical wake scaling method to measured nominal fields at model scale, and observed noticeable differences.

2 METHODS

2.1 Boundary Element Method for Propeller Analysis

A potential-based boundary element method ("panel code") serves as the main tool for propeller analysis in the present work. As for all potential flow-based methods, inviscid, incompressible, and irrotational flow is assumed. Sheet cavitation is modeled in a partially nonlinear way. The present implementation's approach to cavitation modeling – whose basic formulation is reproduced below – follows the approach initially described by Fine (1992) and is able to predict unsteady sheet cavitation in inhomogeneous inflow, including supercavitation.

The velocity potential must satisfy the Laplace equation:

$$\nabla^2 \Phi = 0 \tag{1}$$

Given the linearity of Eq. (1), the total velocity potential Φ can be split into a known onset part ϕ_{Onset} (dependent on the wake field with the local velocity $\boldsymbol{U}_{\text{Wake}}$ and the propeller rotation, the sum of those resulting in a local velocity vector $\boldsymbol{U}_{\text{Onset}} = \nabla\phi_{\text{Onset}}$) and a propeller geometry-dependent perturbation potential ϕ that is to be determined.

$$\Phi = \phi_{\text{Onset}} + \phi \tag{2}$$

For a domain bound by the blade surface S_B (with a continuous distribution of sources and dipoles) and the force-free wake surface S_W (with a continuous distribution of dipoles), application of Green's second identity gives the potential at a field point p, when the integration point q lies on the domain boundary. G is defined as the inverse of the distance R between these two points, $G = \frac{1}{R}$. The term $\Delta\phi_q$ corresponds to the potential jump across the wake sheet at an integration point q on S_W. An additional term appears in the presence of supercavitation, as additional sources are placed on the cavitating part of the wake, $S_{CW} \subset S_W$.

If the field point p lies on the blade surface, the potential ϕ_p is found from

$$\begin{aligned} 2\pi\phi_p = &\int_{S_B} \left[\phi_q \frac{\partial G}{\partial n} - G\frac{\partial \phi_q}{\partial n}\right] dS \\ &- \int_{S_{CW}} \left[G\Delta\frac{\partial \phi_q}{\partial n}\right] dS \\ &+ \int_{S_W} \left[\Delta\phi_q \frac{\partial G}{\partial n}\right] dS \end{aligned} \tag{3}$$

As the surface S_W in principle consists of two surfaces collapsed into one infinitely thin wake sheet, the integral equation reads slightly differently if the field point lies on S_W. The potential ϕ_p for a field point on the wake surface is

$$\begin{aligned} 4\pi\phi_p = &2\pi\Delta\phi_q \\ &+ \int_{S_B} \left[\phi_q \frac{\partial G}{\partial n} - G\frac{\partial \phi_q}{\partial n}\right] dS \\ &- \int_{S_{CW}} \left[G\Delta\frac{\partial \phi_q}{\partial n}\right] dS \\ &+ \int_{S_W} \left[\Delta\phi_q \frac{\partial G}{\partial n}\right] dS \end{aligned} \tag{4}$$

Equations (3) and (4) are then discretized using flat quadrilateral panels arranged in a structured mesh. Introducing influence coefficient matrices $\boldsymbol{A}$ through $\boldsymbol{H}$ that describe the influence from unit strength singularities located on panel j on the control point of panel i, a system of $J_B + J_{CW}$ equations and unknowns results. For each panel on the blade one equation of the following form exists

$$\begin{aligned} 2\pi\phi_i = &\sum_{J_B} (-\phi_j \boldsymbol{A}_{ij}) + \sum_{J_B} (\sigma_j \boldsymbol{B}_{ij}) \\ &+ \sum_{J_{CW}} (\sigma_j \boldsymbol{C}_{ij}) \quad - \sum_{J_W} (\Delta\phi_j \boldsymbol{G}_{ij}) \end{aligned} \tag{5}$$

and for each cavitating wake panel there is an additional equation of the form

$$\begin{aligned} 4\pi\phi_i = &\sum_{J_B} (-\phi_j \boldsymbol{D}_{ij}) + \sum_{J_B} (\sigma_j \boldsymbol{E}_{ij}) \\ &+ \sum_{J_{CW}} (\sigma_j \boldsymbol{F}_{ij}) \quad - \sum_{J_W} (\Delta\phi_j \boldsymbol{H}_{ij}) \\ &+ 2\pi\Delta\phi_j \end{aligned} \tag{6}$$

On the wetted part of the blade, the source strengths $\sigma_i = \frac{\partial \phi}{\partial n}$ are known from the kinematic boundary condition, Eq. (7),

and the dipole strength is the unknown.

$$\nabla\Phi\cdot\boldsymbol{n}=\boldsymbol{U}_{\text{Onset}}\cdot\boldsymbol{n}+\frac{\partial\phi}{\partial n}=0$$
$$\frac{\partial\phi}{\partial n}=-\boldsymbol{U}_{\text{Onset}}\cdot\boldsymbol{n} \tag{7}$$

On the cavitating part of the blade and wake surfaces, a dynamic boundary condition is applied, prescribing the pressure to correspond to the given cavitation number σ_n. To achieve this, the corresponding local "cavity velocity" needs to be found. For convenience, this part is formulated in curvilinear coordinates aligned with the panel edges. The v-direction is pointing outwards in spanwise direction and the s-direction is the chordwise direction, positive towards the trailing edge on the suction side of the blade. The angle between the $\hat{s}$ and $\hat{v}$ vectors of a panel is designated θ and is usually close to 90°. With U_s and U_v as the s- and v-components of the onset velocity vector and z as the vertical distance from the propeller shaft, the chordwise cavity velocity corresponding to the cavitation number σ_n at shaft depth is

$$\frac{\partial\phi}{\partial s}=-U_s + \cos(\theta)\left(\frac{\partial\phi}{\partial v}+U_v\right)+\sin(\theta)\sqrt{f} \tag{8}$$

where

$$f=(nD)^2\sigma_n+|\boldsymbol{U}_{\text{Onset}}|^2-\left(\frac{\partial\phi}{\partial v}+U_v\right)^2 - 2\frac{\partial\phi}{\partial t}-2gz \tag{9}$$

To be able to provide a Dirichlet boundary condition on the potential, Eq. (8) is integrated in chordwise direction and added to the potential at the chordwise detachment point ϕ_0, which is assumed known and practically expressed by extrapolation from the wetted part ahead of the cavity.

$$\phi=\phi_0+\int_0^{s_p}\frac{\partial\phi}{\partial s}\mathrm{d}s \tag{10}$$

The cavity extent on the blade (and wake) needs to be found iteratively. After an initial guess based on the non-cavitating pressure distribution and cavitation number, the cavity thickness is computed. The cavity extent is then changed until the cavity thickness is sufficiently close to zero at the edges of the cavity sheet, so it detaches from the blade and closes on the blade or wake.

The approach to cavitation modeling within a panel method described above goes back to the formulation by Fine (1992). The present implementation also includes additional features described by Fine (ibid.), such as the split panel technique for faster convergence and more flexibility in terms of mesh and timestep size. However, the present implementation, the DTU-developed panel code "ESPPRO", uses lower order extrapolation schemes throughout for increased numerical stability. Also, spatial derivatives in the cavity height equation are discretized using lower order finite differences.

2.2 RANS-BEM Coupling

In recent years, viscous flow simulations around the hull coupled with potential flow-based propeller models have become a popular choice for numerical self-propulsion simulations. Usually field methods solving the Reynolds-averaged Navier–Stokes equations are used for the hull part, and panel methods (boundary element methods) are a common choice for the propeller calculations, as they allow for a decent representation of the flow physics while only requiring limited computational effort. Computational approaches using this combination of tools are then often referred to as "RANS-BEM Coupling".

In such an approach, the exact propeller geometry is not resolved in CFD, but the propeller is accounted for by modeling its effect on the flow by introducing body forces, provided by the propeller model. This is an iterative process: The total velocity field in the coupling plane (an approximation of the propeller plane) is passed from the RANS solver to the propeller model, which then returns the propeller forces that correspond to this inflow field. The key part here is that the inflow field to the propeller model is not the total wake field as extracted from the global CFD simulation, but rather the effective wake field, i.e. with the propeller induced velocities subtracted from the total wake field. The induced velocity field is approximated by using the values from the previous coupling iteration. Thereby, the effective wake field is not only a byproduct but also an inherent part of this iterative coupling.

By being able to compute not only the effective wake *fraction* but also the *distribution* of the effective wake velocities in the propeller disk, the RANS-BEM coupling approach provides a major advantage over all-CFD simulations beyond substantially reducing the computational effort.

In the present work, the RANS-BEM coupling approach is used to determine effective wake fields at model and full scale to later investigate differences in propeller cavitation.

On the RANS side, the XCHAP solver from the commercial SHIPFLOW package is used. XCHAP solves the steady-state RANS equations on overlapping, structured grids using the finite volume method and employs the EASM (Explicit Algebraic Stress Model) turbulence model. Nominal wake fields are found using the same RANS solver and identical grids, but with the propeller model switched off.

The DTU-developed panel code ESPPRO (whose basic formulation is described in the previous section) serves as the propeller model. To reduce computational effort, the non-cavitating condition is assumed in self-propulsion and the cavitation model described previously remains disabled. The unsteady propeller forces are time-averaged over one revolution before being passed to XCHAP. In line with that, the induced velocity field is also time-averaged to compute the effective wake field in the subsequent coupling iteration.

Previous work on computing effective wake fields using RANS-BEM coupling by Rijpkema et al. (2013) highlighted the importance and influence of the location of the coupling plane on self-propulsion results. As singularities are placed on the propeller blade surfaces in the panel method, the induced velocities can not be computed in the propeller plane

directly. To avoid evaluating induced velocities too close to the singularities, the coupling plane is usually chosen to be upstream of the propeller. Extrapolating the effective wake to the propeller plane linearly from two upstream planes was found to give best results in terms of predicting the self-propulsion point (effective wake fraction in self-propulsion) by Rijpkema et al. (ibid.).

For the present work, the distribution of effective velocities in the coupling plane is of higher interest than the mean velocity, i.e. the absolute value of the wake fraction. Therefore, and to remove any potential extrapolation artifacts that affect the distribution, the effective wake is computed on a single curved surface that follows the blade leading edge contour closely (at a distance of 2% of the propeller diameter), essentially resulting in a curved coupling plane just upstream of the propeller.

3 APPROACH

All calculations are carried out for a state-of-the-art handy-size bulk carrier, representing a modern single-screw full hull form. The block coefficient is 0.82 and the aftbody is of pram-with-gondola-type. In this work, nominal wake fields at model and full scale for this ship are obtained by running steady-state RANS-based CFD simulations. Effective wake fields at the self-propulsion point, also at both model and full scale, are computed using the hybrid RANS-BEM method described in the previous section. Additionally, Sasajima's wake scaling method is applied to the model scale nominal wake field for comparison with the computed full scale fields.

Using the panel code with the cavitation model described in Section 2.1, the effect of the wake distribution on propeller cavitation performance, including cavitation extent, cavitation volume, and hull pressure pulses, is examined.

For that purpose, a simple conventional propeller is designed for the bulk carrier mentioned above. The effective wake fraction determined from self-propulsion experiments with a stock propeller is $w = 0.25$. Resistance and thrust deduction values from the experiment establish the thrust requirement for the propeller design. The propeller for this ship is moderately loaded ($C_{TH} = 1.4$) at the design point.

For the propeller design, a lifting line-based propeller design tool is employed that finds the optimum radial load (circulation) distribution for a circumferentially averaged wake field. Radial pitch and camber distributions can then be found from the circulation distribution, assuming a standard NACA66 profile. Based on the designer's experience, the propeller was chosen to be 3-bladed with moderate skew and no rake. The expanded blade area ratio was selected as $A_E/A_0 = 0.3$.

The nominal wake field obtained from SHIPFLOW-XCHAP is circumferentially averaged and scaled to the effective wake fraction found from the experiment. This averaged and scaled nominal wake field at model scale (see Fig. 1) is then used as input for the design. The optimum radial distribution of circulation found from lifting line theory for this case is shown in Fig. 2. The corresponding propeller is from now on referred to as Propeller "M".

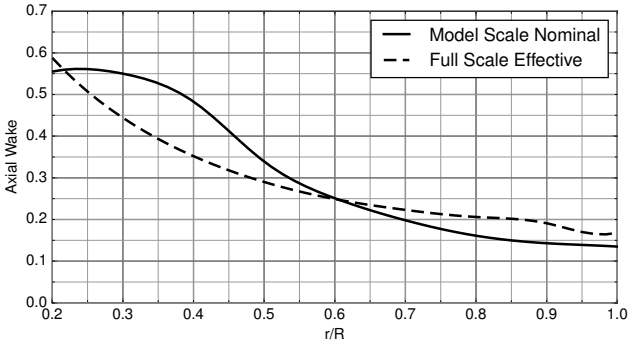

Figure 1: Circumferentially Averaged Axial Velocities

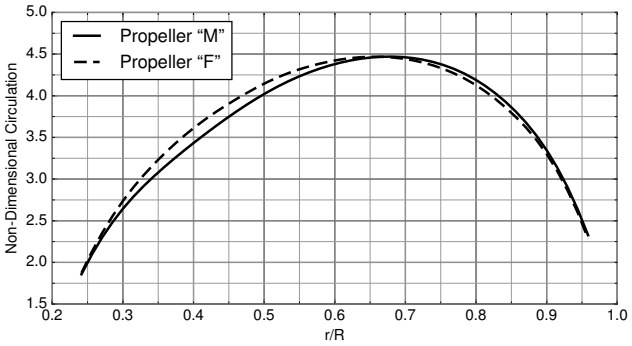

Figure 2: Radial Circulation Distributions

Using this propeller, numerical self-propulsion simulations are carried out to find the effective wake fields at model and full scale, using the method described in Section 2.2.

Based on the full scale effective wake as input, the propeller design process is then repeated, yielding Propeller "F". Other input parameters, such as number of blades and blade area ratio, remain unchanged. The circumferentially averaged axial inflow for this case and the resulting radial circulation distribution are shown as dashed lines in Fig. 1 and 2. An inward shift of the loading compared to Propeller "M" – corresponding to the difference in inflow – can be seen from the latter.

For the cavitation analyses, the axial components of all five wake fields (nominal and effective at model and full scale, plus the result of Sasajima's scaling method) are then uniformly scaled to match $w = 0.25$, so the propeller is running at the same operating point in all wake fields. Any differences in results are then due to the different velocity *distributions* in the propeller disk and different in-plane velocity components.

All cavitation simulations are carried out at a cavitation number (based on the propeller speed n) of $\sigma_n = 1.8$, corresponding to the full scale condition.

4 RESULTS AND DISCUSSION

4.1 Wake Fields

Figures 3a–d show the nominal and effective wake distributions based on the RANS and RANS-BEM results. Figure 3e shows the full scale wake field after applying Sasajima's scaling method, based on the computed nominal wake at model scale and the potential wake (see Fig. 4), computed using the panel code SHIPFLOW-XPAN.

A strong bilge vortex can be seen in Fig. 3a, which results in low axial velocities in the region between the hub and 40% of the propeller radius. It should be noted that for these radii the axial velocities are actually higher in the usual "wake peak" region between 330° and 30°.

Looking at the effective wake distribution resulting from the self-propulsion simulation at model scale, Fig. 3b, the bilge vortex appears substantially weaker and closer to the centerline. This is also obvious from the radial and tangential velocity components which are otherwise of similar magnitude as in Fig. 3a. The effective field shown in Fig. 3b exhibits a much more defined and pronounced wake peak at 12 o'clock, the axial velocities reaching consistently low values in this region.

The asymmetric flow at the innermost radii seen in Fig. 3b is attributed to the lack of the propeller hub in both the RANS and the BEM part of the simulation. No propeller shaft, hub, or even stern tube was part of the RANS grids. The lack of the hub in the propeller panel code results in an unrealistic flow around the open blade root. Consequently, secondary flow structures emerge at low Reynolds numbers. While undesirable, the effect is local and is not expected to influence the cavitation behavior. As can be seen in Fig. 3d, this is of less concern at full scale.

Moving to full scale, the nominal wake distribution (Fig. 3c) changes significantly compared to model scale, as expected. The bilge vortex is remarkably less dominant, and the isolines of the axial wake distribution are more U-shaped. With a thinner boundary layer and a weaker bilge vortex, the in-plane velocity components change as well. In both computed full scale fields, the radial and tangential components indicate a less vortical and more upwards-directed flow. Except for the remainders of the bilge vortex, the in-plane velocity distribution approaches the potential one (Fig. 4).

The trend towards a more defined and narrower wake peak continues moving on to the effective wake distribution at full scale, shown in Fig. 3d. A bilge vortex can hardly be observed anymore.

Applying the method by Sasajima & Tanaka (1966) leads to a very different wake distribution. The method works by contracting the nominal model scale wake field horizontally while also scaling the axial velocities, depending on the relationship of frictional and potential wake. For this particular case – with the above-described flow features in the nominal wake field at model scale – this results in a box-shaped region of very low axial velocities, visible in Fig. 3e. Given that all fields shown in Fig. 3 are uniformly scaled to the same wake fraction, the velocities in the outer and lower regions are very high, compensating for the large low-velocity region described previously.

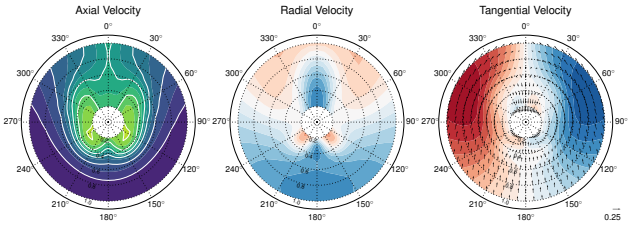

(a) Nominal Wake Distribution – Model Scale

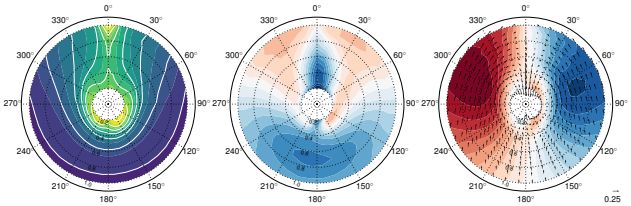

(b) Effective Wake Distribution – Model Scale

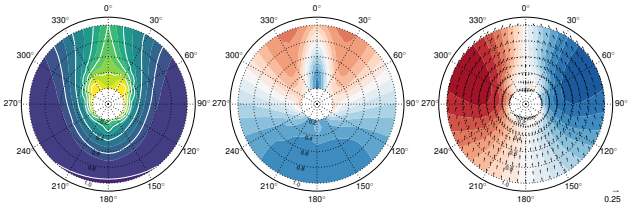

(c) Nominal Wake Distribution – Full Scale

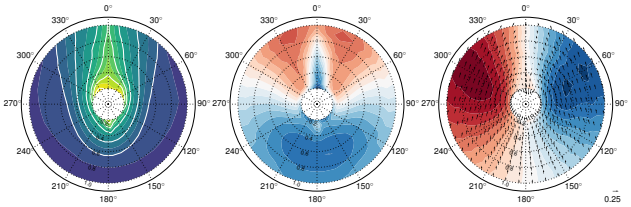

(d) Effective Wake Distribution – Full Scale

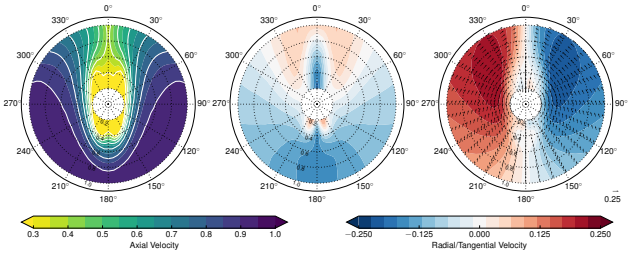

(e) Wake Distribution – Sasajima Scaling

Figure 3: Wake Fields for Cavitation Analysis ($w = 0.25$)

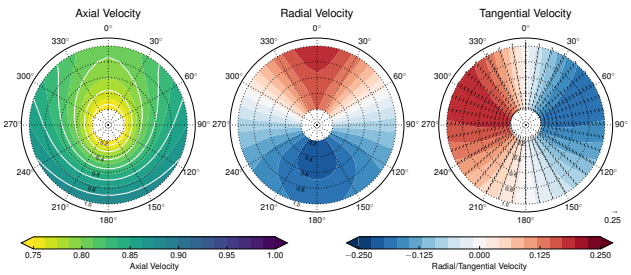

Figure 4: Potential Wake Field

4.2 Sheet Cavitation

The unsteady sheet cavitation on Propeller "M" and Propeller "F" was analyzed in the five wake fields shown in Fig. 3 using ESPPRO, the panel code for propeller analysis described in Section 2.1. As mentioned before, the input to the simulations differed only in the wake distribution. Wake fraction, cavitation number, scale, and all other parameters are identical across all cases presented below.

Figure 5 gives an overview over the global differences in sheet cavitation over one revolution for Propeller "M" and Propeller "F". The lines indicate the radial extent of sheet cavitation for all blade angles in the different wakes. The lower cutoff threshold for these plots is a cavity thickness of 5% of the blade section thickness at $r/R = 0.7$.

As can be seen from Fig. 5a, there is some variation in terms of the cavitation inception angle (between 340° and 350°) and significant disagreement in terms of radial extent for Propeller "M" in the five wake fields. The nominal wake distribution at model scale clearly results in the smallest cavitation extent, underpredicting the extent seen in the full scale effective field significantly. Using the full scale distribution obtained by Sasajima's method, the extent is overpredicted by a similar margin, which is not surprising given the wake field seen in Fig. 3e. The other three curves – representing the effective distribution at model scale and the two full scale fields – result in remarkably similar extents.

The variation in cavitation extent is more easily quantified by looking at the cavity volume on one blade (non-dimensionalized by D^3), as shown in Fig. 6 for Propeller "M". Confirming the general trends between the wakes visible in Fig. 5a, the differences in inception and closure angle appear more clearly from Fig. 6. The plot also indicates that the time-derivatives of the cavity volume are rather different when the cavity is shrinking between approx. 15°–70° blade angle. Disregarding the curve corresponding to the field scaled by Sasajima's method, particularly large differences exist comparing the results based on the nominal model scale distribution to the other computed curves. In that inflow field, the maximum cavity volume on Propeller "M" is 30% smaller than for the same propeller in the full scale effective distribution. Also, the first and second derivatives of the cavity volume appear to be considerably different, the nominal model scale distribution again resulting in the smallest – and least conservative – values.

Hull pressure pulses were evaluated in a single point, located on the centerline, 17% of the propeller diameter above the propeller plane. These calculations were done in the BEM part of the simulation, applying the Bernoulli equation at an offbody point and Fourier-transforming the time signal. The results for Propeller "M" are given in Tab. 1, which shows first and second harmonics of the blade frequency, normalized by the results for the nominal model scale distribution. The pressure pulse results also reflect the findings described previously. For example, in the full scale effective wake distribution the value for the first harmonic is 17% larger compared to the nominal distribution at model scale. The differences are even larger for the second harmonic. Higher harmonics have not been evaluated as the driving factors, such as tip vortex cavitation, are not captured or modeled in the present propeller analysis method.

It can be seen from Fig. 5b as well as Fig. 7 that the characteristics of sheet cavitation extent and behavior of Propeller "F" are generally similar to Propeller "M". The magnitude of all values, however, is significantly lower. The cavitation volume in the full scale effective distribution is reduced by about 40%, compared to Propeller "M". Corresponding reductions in pressure pulses appear from Tab. 2. Note that the values in that table are still relative to the nominal model scale results for Propeller "M" (see Tab. 1).

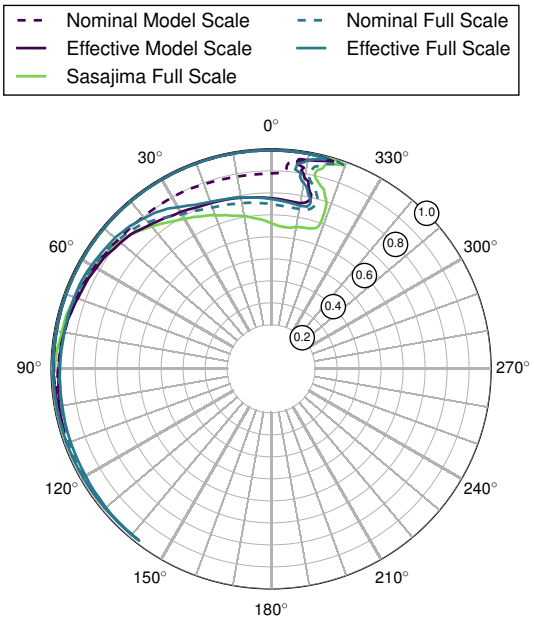

(a) Propeller "M"

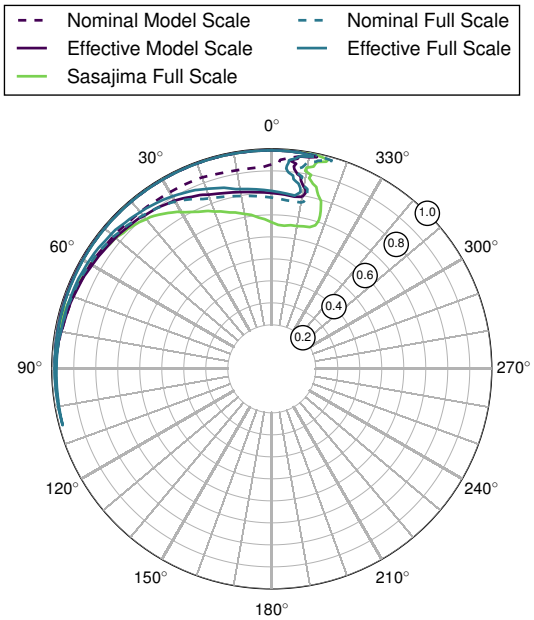

(b) Propeller "F"

Figure 5: Cavitation Extent in Different Wakes

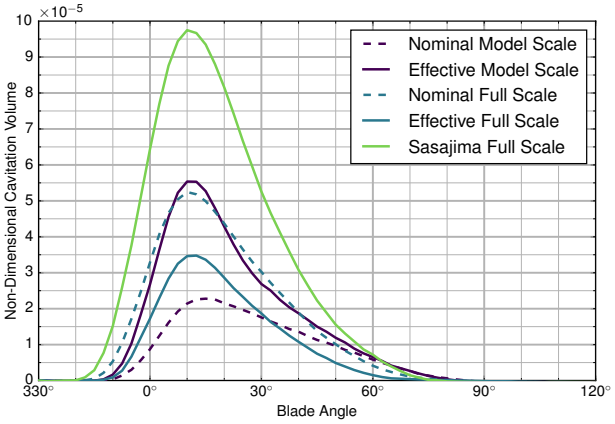

Figure 6: Cavitation Volume, Propeller "M"

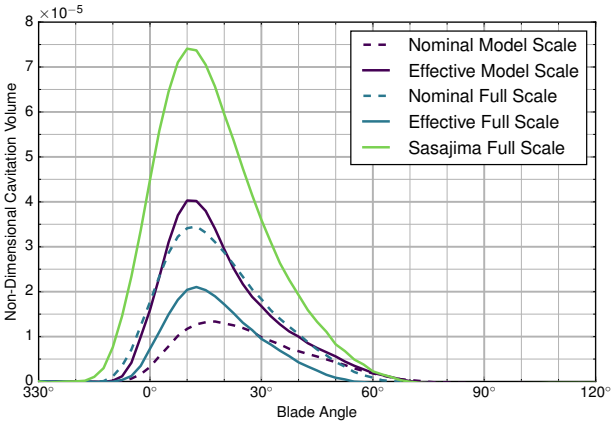

Figure 7: Cavitation Volume, Propeller "F"

Table 1: Pressure Pulse Harmonics, Propeller "M"

Wake Distribution	1st Harm.	2nd Harm.
Nominal Model Scale	100%	100%
Effective Model Scale	125%	186%
Nominal Full Scale	131%	182%
Effective Full Scale	117%	158%
Sasajima Full Scale	173%	243%

Table 2: Pressure Pulse Harmonics, Propeller "F"

Wake Distribution	1st Harm.	2nd Harm.
Nominal Model Scale	86%	80%
Effective Model Scale	107%	161%
Nominal Full Scale	112%	163%
Effective Full Scale	101%	134%
Sasajima Full Scale	149%	218%

5 CONCLUSIONS

For the examined case of a modern and representative full-form ship, using the model scale nominal wake distribution for propeller design and cavitation analysis leads to a significant underprediction of cavitation extent, volume, and pressure pulses, compared to the behavior of the same propeller in the full scale effective wake field. Therefore, a conservative design is required if the propeller designer only has access to the measured nominal wake field. Otherwise the expected extent of cavitation and acceptable levels of pressure pulses might be exceeded in full scale.

Compared to the propeller designed on the basis of the nominal wake in model scale, the propeller designed for the effective full scale wake distribution performs better in all cavitation criteria considered. This highlights the importance of accurate wake data and the benefits of those – or hull geometry information – being available to the propeller designer. Knowing the effective wake distribution at full scale allows for a more realistic cavitation prediction in the propeller design process, enabling more efficient propeller designs.

REFERENCES

Fine, N. E. (1992). Nonlinear Analysis of Cavitating Propellers in Nonuniform Flow. Ph.D. thesis, Massachusetts Institute of Technology.

Fu, T. C., Takinaci, A. C., Bobo, M. J., Gorski, W., Johannsen, C., Heinke, H.-J., Kawakita, C. & Wang, J.-B. (2011). 'Final Report of The Specialist Committee on Scaling of Wake Field'. Proceedings of the 26th ITTC, vol. II, pp. 379–417. International Towing Tank Conference, Rio de Janeiro.

Gaggero, S., Villa, D., Viviani, M. & Rizzuto, E. (2014). 'Ship wake scaling and effect on propeller performances'. Developments in Maritime Transportation and Exploitation of Sea Resources, pp. 13–21. CRC Press, London.

Jessup, S., Mewis, F., Bose, N., Dugue, C., Esposito, P. G., Holtrop, J., Lee, J.-T., Poustoshny, A., Salvatore, F. & Shirose, Y. (2002). 'Final Report of the Propulsion Committee'. Proceedings of the 23rd ITTC, vol. I, pp. 89–151. International Towing Tank Conference, Venice.

Rijpkema, D., Starke, B. & Bosschers, J. (2013). 'Numerical simulation of propeller-hull interaction and determination of the effective wake field using a hybrid RANS-BEM approach'. 3rd International Symposium on Marine Propulsors (smp'13), pp. 421–429. Launceston, Australia.

Sasajima, H. & Tanaka, I. (1966). 'Report of the Performance Committee, Appendix X: On the Estimation of Wake of Ships'. Proceedings of the 11th ITTC, pp. 140–144. International Towing Tank Conference, Tokyo.